Journal of Biomolecular NMR (2020) 74:695–706
https://doi.org/10.1007/s10858-020-00341-x

ARTICLE

Sensitive and simplified: a combinatorial acquisition of five distinct 2D constant-time $^{13}C-^{1}H$ NMR protein correlation spectra

Yuichi Yoshimura[1,2,3] · **Frans A. A. Mulder**[4]

Received: 26 June 2020 / Accepted: 12 August 2020 / Published online: 17 August 2020

Abstract

A procedure is presented for the substantial simplification of 2D constant-time $^{13}C-^{1}H$ heteronuclear single-quantum correlation (HSQC) spectra of ^{13}C-enriched proteins. In this approach, a single pulse sequence simultaneously records eight sub-spectra wherein the phases of the NMR signals depend on spin topology. Signals from different chemical groups are then stratified into different sub-spectra through linear combination based on Hadamard encoding of $^{13}CH_n$ multiplicity ($n = 1$, 2, and 3) and the chemical nature of neighboring ^{13}C nuclei (aliphatic, carbonyl/carboxyl, aromatic). This results in five sets of 2D NMR spectra containing mutually exclusive signals from: (i) $^{13}C^{\beta}-^{1}H^{\beta}$ correlations of asparagine and aspartic acid, $^{13}C^{\gamma}-^{1}H^{\gamma}$ correlations of glutamine and glutamic acid, and $^{13}C^{\alpha}-^{1}H^{\alpha}$ correlations of glycine, (ii) $^{13}C^{\alpha}-^{1}H^{\alpha}$ correlations of all residues but glycine, and (iii) $^{13}C^{\beta}-^{1}H^{\beta}$ correlations of phenylalanine, tyrosine, histidine, and tryptophan, and the remaining (iv) aliphatic $^{13}CH_2$ and (v) aliphatic $^{13}CH/^{13}CH_3$ resonances. As HSQC is a common element of many NMR experiments, the spectral simplification proposed in this article can be straightforwardly implemented in experiments for resonance assignment and structure determination and should be of widespread utility.

Keywords ^{13}C chemical shifts · Constant-time HSQC · Multiplicity editing · Scalar coupling · Selective observation

Introduction

Among a variety of multi-dimensional NMR experiments for studies of proteins, two-dimensional (2D) heteronuclear single-quantum correlation (HSQC) experiments (Bodenhausen and Ruben 1980; Bax et al. 1990) are commonly used on ^{13}C- and ^{15}N-enriched proteins. A 2D $^{15}N-^{1}H$ HSQC experiment is expected to provide one backbone amide resonance for each amino acid residue (except for proline) of the protein, where the signals in the spectrum are usually well-dispersed and well-resolved for small folded proteins. It is also possible to separate between backbone ^{15}NH and side-chain $^{15}NH_2$ signals of proteins (Kay and Bax 1989; Schmidt and Rueterjans 1990; Tate et al. 1991). The experiment is often performed in protein interaction studies as chemical shift changes in the protein can be readily observed (Zuiderweg 2002; Williamson 2013). In contrast, a 2D $^{13}C-^{1}H$ HSQC experiment detects all backbone and side-chain $^{13}C-^{1}H$ moieties, and the spectrum is usually less resolved in comparison with 2D $^{15}N-^{1}H$ HSQC. High resolution in the ^{13}C dimension is therefore required to alleviate resonance overlap in the crowded spectrum, and for effective decoupling of homonuclear one-bond $^{13}C-^{13}C$ couplings

Electronic supplementary material The online version of this article (https://doi.org/10.1007/s10858-020-00341-x) contains supplementary material, which is available to authorized users.

✉ Frans A. A. Mulder
fmulder@chem.au.dk

Yuichi Yoshimura
yyoshimura@protein.osaka-u.ac.jp

1 Lifematics West-Japan Branch, Hirano-machi 4-6-16, Chuo-ku, Osaka 541-0046, Japan

2 Institute for Protein Research, Osaka University, Yamada-oka 3-2, Suita, Osaka 565-0871, Japan

3 Program of Mathematical and Life Sciences, Graduate School of Integrated Sciences for Life, Hiroshima University, Kagamiyama 1-3-1, Higashi-Hiroshima, Hiroshima 739-8526, Japan

4 Department of Chemistry and Interdisciplinary Nanoscience Center (iNANO), Aarhus University, Gustav Wieds Vej 14, 8000 Aarhus C, Denmark

that limit spectral resolution, a constant-time (CT) chemical shift evolution scheme (Santoro and King 1992, van de Ven and Philippens 1992, Vuister and Bax 1992) is extensively used. However, resonance overlap in the 2D CT $^{13}C-^{1}H$ HSQC spectrum that complicates spectral interpretation is still significant even for proteins as small as ubiquitin (76 amino acid residues) used in this study.

Several types of multiplicity-based editing of NMR signals have been proposed for spectral simplification. The one-bond $^{13}C-^{1}H$ couplings ($^{1}J_{CH}$) have been used to separate $^{13}CH_2$ signals from ^{13}CH and $^{13}CH_3$ signals (Bendall et al. 1981). The ^{13}C DEPT is routinely used in the field of organic chemistry for differentiation between ^{13}CH, $^{13}CH_2$, and $^{13}CH_3$ groups (Doddrell et al. 1982). These techniques have been then applied to multi-dimensional experiments (Kessler et al. 1989; Davis 1990, 1991; Nagana Gowda 2002; Chen et al. 2015; Sakhaii and Bermel 2015). Moreover, selective observation of aliphatic ^{13}C ($^{13}C_{ali}$) carbons adjacent to a carbonyl/carboxyl (^{13}CO) and an aromatic ($^{13}C_{aro}$) carbon in ^{13}C-enriched proteins can be achieved by spectral editing with the one-bond couplings between the $^{13}C_{ali}$ and ^{13}CO carbons ($^{1}J_{CCO}$) and between the $^{13}C_{ali}$ and $^{13}C_{aro}$ carbons ($^{1}J_{CCaro}$), respectively (Grzesiek and Bax 1993). Furthermore, several sophisticated multiplicity-dependent coherence transfer schemes in triple ($^{1}H/^{13}C/^{15}N$) resonance experiments are proposed for selecting amino acid types based on the particular chemical shifts and spin coupling topologies of the side-chains (Tashiro et al. 1995; Feng et al. 1996; Rios et al. 1996; Schubert et al. 1999, 2001a, b, 2005; Van Melckebeke et al. 2004; Lescop et al. 2008; Pantoja-Uceda and Santoro 2008; Feuerstein et al. 2012; Brenner and Frøystein 2014; Dubey et al. 2016).

While selection of desired coherence pathways can be useful for unambiguous resonance assignments in protein NMR spectroscopy, it often requires additional coherence transfer steps that cause a significant reduction in sensitivity, and besides, different spectra need to be obtained as such tailored experiments select only desired coherences for specific amino acid residues. On the other hand, experiments with sign encoding provides signals for all amino acid residues simultaneously, thereby increasing the sensitivity of the method. Brutscher and coworkers have proposed the use of a Hadamard-based sign encoding scheme to discriminate among amino acid types in a 2D $^{15}N-^{1}H$ correlation experiment (Lescop et al. 2008; Feuerstein et al. 2012) and in 2D and 3D methyl NOESY experiments (Van Melckebeke et al. 2004).

Separation of NMR signals based on multiplicity can be achieved by means of collecting sub-spectra; The experiment is recorded twice, once where a particular *J*-coupling evolution is active such that the signal is inverted, and once where it is not. Summation of the two sub-spectra will lead to cancellation of the particular signal, whereas subtraction will restore its full intrinsic intensity. Importantly, full signal intensity for all signals is registered every time, and the unscrambling for a given peak is obtained from a straightforward linear combination (*vide infra*). For example, a $^{13}CH_n$ multiplicity-based experiment ($n = 1$, 2, and 3) can be recorded with or without $^{1}J_{CH}$ evolution active during the editing period of $1/^{1}J_{CH}$. This will result in two spectra where the phases of the ^{13}CH and $^{13}CH_3$ signals are opposite for the two repetitions of the experiment, whereas the sign for the $^{13}CH_2$ signals is unchanged. The addition and subtraction of the two sub-spectra then yields two complementary spectra with only $^{13}CH_2$ or $^{13}CH/^{13}CH_3$ concurrently (Chen et al. 2015). In 2D CT $^{13}C-^{1}H$ HSQC experiments on ^{13}C-enriched proteins, signals of $^{13}C_{ali}$ attached to ^{13}CO and $^{13}C_{aro}$ carbon can be separated in a similar manner utilizing $^{1}J_{CCO}$ and $^{1}J_{CCaro}$ couplings (Grzesiek and Bax 1993). The editing period with the $^{1}J_{CCO}$ (or $^{1}J_{CCaro}$) coupling renders opposite the signals for ^{13}CO-coupled (or $^{13}C_{aro}$-coupled) $^{13}C_{ali}$ carbons in the two sub-spectra, and the difference spectrum separates their signals from the others.

This study aims at separating NMR signals of ^{13}C-enriched proteins in a 2D CT $^{13}C-^{1}H$ HSQC experiment by means of combinatorial sign-encoding of the following three couplings: $^{1}J_{CH}$, $^{1}J_{CCO}$, and $^{1}J_{CCaro}$. Eight sub-spectra are collected with the binary editing (i.e. *J*-active or *J*-inactive) schemes for each of the three couplings. A linear combination of sums and differences of these eight sub-spectra using a Hadamard matrix generates a series of multiplicity-separated NMR spectra. Because all three editing periods, $1/^{1}J_{CH}$, $1/^{1}J_{CCO}$, and $1/^{1}J_{CCaro}$, are incorporated into the CT $^{13}C_{ali}$ chemical shift evolution period without any additional delays, no additional relaxation loss is produced in comparison with the corresponding unedited 2D CT $^{13}C-^{1}H$ HSQC experiment. The strategy proposed in this article, hereinafter referred to as OROCHI (***O***rthogonal ***R***egistration ***O***f ***C***onstant-time ***H***SQC ***I***ntensities), allows selective observation of the following classes of complementary NMR signals:

I. Aliphatic $^{13}CH_2$ resonances whose ^{13}C carbon is not coupled to a carbonyl, carboxyl, or aromatic ^{13}C carbon
II. Aliphatic $^{13}CH/^{13}CH_3$ resonances whose ^{13}C carbon is not coupled to a carbonyl, carboxyl, or aromatic ^{13}C carbon
III. $^{13}C^{\beta}-^{1}H^{\beta}$ correlations of asparagine and aspartic acid (Asx), $^{13}C^{\gamma}-^{1}H^{\gamma}$ correlations of glutamine and glutamic acid (Glx), and $^{13}C^{\alpha}-^{1}H^{\alpha}$ correlations of glycine
IV. $^{13}C^{\alpha}-^{1}H^{\alpha}$ correlations of all residues except for glycine
V. $^{13}C^{\beta}-^{1}H^{\beta}$ correlations of phenylalanine, tyrosine, histidine, and tryptophan (F/Y/H/W)

Materials and methods

NMR experiments were performed on uniformly ^{13}C-labelled human ubiquitin. Ubiquitin (5 mg as lyophilized powder) was purchased from Taiyo Nippon Sanso (Tokyo, Japan) and was dissolved at a protein concentration of 1 mM into D_2O (0.55 mL) containing 50 µM sodium 2,2-dimethylsilapentane-5-sulfonate (DSS) as chemical shift reference (Markley et al. 1998). Unless otherwise indicated, NMR data were acquired at 298 K with a Bruker spectrometer at the magnetic field of 11.7 T (i.e. ^{1}H frequency of 500 MHz) equipped with a cryogenic BBO probe, and were processed with the Bruker Topspin 3.6.2 and NMRPipe (Delaglio et al. 1995). Spectral assignment of ubiquitin was taken from BMRB entries 5387 and 17769 (http://www.bmrb.wisc.edu/).

In the 2D CT ^{13}C−^{1}H HSQC experiments, the homonuclear one-bond ^{13}C−^{13}C couplings between $^{13}C_{ali}$ carbons (herein written $^1J_{CC}$) are active during the entire CT period $2T_C$ (between points *b* and *c* in Fig. 1a, b) whereas the $^{13}C_{ali}$ chemical shift evolves for $t_1/2+T_C-(T_C-t_1/2)=t_1$. The first INEPT step converts the initial magnetization to the longitudinal two-spin order term $2H_zC_z$ (point *a* in Fig. 1a,b) (Morris and Freeman 1979), and at time point *b*, the $^{13}C_{ali}$ anti-phase $2H_zC_y$ (or $-2H_zC_y$, depending on the phase of ϕ_1) magnetization is generated. The evolution of the $^{13}C_{ali}$ magnetization during $2T_C$ due to the $^1J_{CC}$ couplings (~35 Hz) for weakly coupled spin systems yields $2H_zC_y\cos^m(2\pi^1J_{CC}T_C)$, where *m* is the number of neighboring $^{13}C_{ali}$ carbons and anti-phase terms with respect to the adjacent $^{13}C_{ali}$ spins are ignored. When $2T_C=1/^1J_{CC}$ (~28 ms), the factor $\cos^m(2\pi^1J_{CC}T_C)$ can be simplified as $(-1)^m$, that is, opposite signs of $^{13}C_{ali}$ magnetization between an even and an odd number of neighboring $^{13}C_{ali}$ carbons are obtained (Santoro and King 1992; Vuister and Bax 1992). However, in common implementations of the CT ^{13}C−^{1}H HSQC experiment signals from $^{13}C_{aro}$-coupled $^{13}CH_2$ and from ^{13}CO-coupled ^{13}CH/$^{13}CH_2$ are strongly attenuated when a broadband pulse is used for inversion of longitudinal magnetization of the coupled ^{13}C nuclei, as can be seen in Fig. 1c. This is so because the $^1J_{CCO}$ (~50–55 Hz) and $^1J_{CCaro}$ (~45–50 Hz) coupling values, listed in Supplementary Tables S1 and S2, are larger than $^1J_{CC}$ (Bystrov 1976). Given that the $^{13}C_{ali}$ magnetization evolution takes place under the $^1J_{CCO}$ or $^1J_{CCaro}$ coupling of $1.5\times{}^1J_{CC}$ (~53 Hz) during the CT period $2T_C=1/^1J_{CC}$, the transfer amplitude of the spin operator, $\cos(2\pi^1J_{CCO}T_C)$ or $\cos(2\pi^1J_{CCaro}T_C)$, will be close to zero. On the other hand, selective inversion of $^{13}C_{ali}$, $^{13}C_{aro}$, and ^{13}CO carbon nuclei with band-selective pulses (see Supplementary Fig. S1) enables refocusing of evolution due to $^1J_{CCO}$ and $^1J_{CCaro}$ couplings, as shown in Fig. 1d, which ensures stronger full sensitivity for the signals of ^{13}CO- and $^{13}C_{aro}$-coupled $^{13}CH_2$ and backbone $^{13}C^{\alpha}$−$^1H^{\alpha}$ correlations. A few example traces from Fig. 1c,d are given in Fig. 1e to demonstrate the extent of sensitivity improvement. Furthermore, spectral editing with $^1J_{CCO}$ and $^1J_{CCaro}$ couplings can be achieved with the band-selective pulses, as will be discussed in the following.

In the OROCHI experiment, a set of the 2D CT ^{13}C−^{1}H HSQC sub-spectra with multiplicity editing were recorded in an interleaved manner using the pulse sequence shown in Fig. 2. For each sub-spectrum, the number of scans was one per indirect (t_1) increment. The corresponding 2D CT ^{13}C−^{1}H HSQC spectrum without multiplicity editing was collected with the pulse sequence shown in Fig. 1b. The ^{1}H carrier frequency was placed at the water resonance (4.8 ppm), and the ^{13}C pulses for $^{13}C_{ali}$, ^{13}CO, and $^{13}C_{aro}$ were centered at 42, 181, and 125 ppm, respectively. Spectral widths were 13 ppm (6.5 kHz) and 80 ppm (10 kHz) for ^{1}H and ^{13}C, respectively. When the CT period, $2T_C$, is set at 28 ms, the spectrum was collected with a matrix size of 512 (^{1}H) × 240 (^{13}C) complex points. When $2T_C=56$ ms, the spectrum was collected with a matrix size of 512 (^{1}H) × 512 (^{13}C) complex points. For sign-encoding of NMR signals based on $^{13}CH_n$ multiplicity, where *n* is the number of protons attached to the $^{13}C_{ali}$ carbon, a set of $^1J_{CH}$-inactive and $^1J_{CH}$-active sub-spectra were recorded. In Fig. 2, the ^{1}H 180° pulse applied during the CT period is indicated in *blue* and *red* for the $^1J_{CH}$-inactive and $^1J_{CH}$-active experiment, respectively. As the net $^1J_{CH}$ evolution time in the $^1J_{CH}$-inactive experiment is $t_1/2-T_C+(T_C-t_1/2)=0$, the phase of the magnetization is unaffected by the $^1J_{CH}$ coupling. In contrast, the net $^1J_{CH}$ evolution time in the $^1J_{CH}$-active experiment is $(t_1/2+\Delta_{CH})-(T_C-\Delta_{CH})+(T_C-t_1/2)=2\Delta_{CH}$, yielding the magnetization $2H_zC_y\cos^n(2\pi^1J_{CH}\Delta_{CH})$. When $2\Delta_{CH}=1/^1J_{CH}$, $\cos^n(2\pi^1J_{CH}\Delta_{CH})$ is equal to $(-1)^n$, generating opposite signs for $^{13}CH_2$ ($n=2$) with respect to ^{13}CH/$^{13}CH_3$ ($n=1$ and 3) signals. Likewise, ^{13}CO- and $^{13}C_{aro}$-attached $^{13}C_{ali}$ carbons were selected utilizing the $^1J_{CCO}$ and $^1J_{CCaro}$ couplings, respectively. In the $^1J_{CCO}$-active (or $^1J_{CCaro}$-active) experiment, where the net $^1J_{CCO}$ (or $^1J_{CCaro}$) evolution time $2\Delta_{CCO}=1/^1J_{CCO}$ (or $2\Delta_{CCaro}=1/^1J_{CCaro}$), the phase of these signals are inverted in comparison with the corresponding $^1J_{CCO}$-inactive (or $^1J_{CCaro}$-inactive) experiment, whereas other $^{13}C_{ali}$ signals are identical. Hadamard matrices were utilized for separation of sign-encoded NMR signals with *k* binary parameters (Kupče et al. 2003; Brutscher 2004). Linear combinations of sums and differences of *N* sub-spectra (from s_1 to s_N), where $N=2^k$, generate a series of multiplicity-separated NMR spectra (from S_1 to S_N):

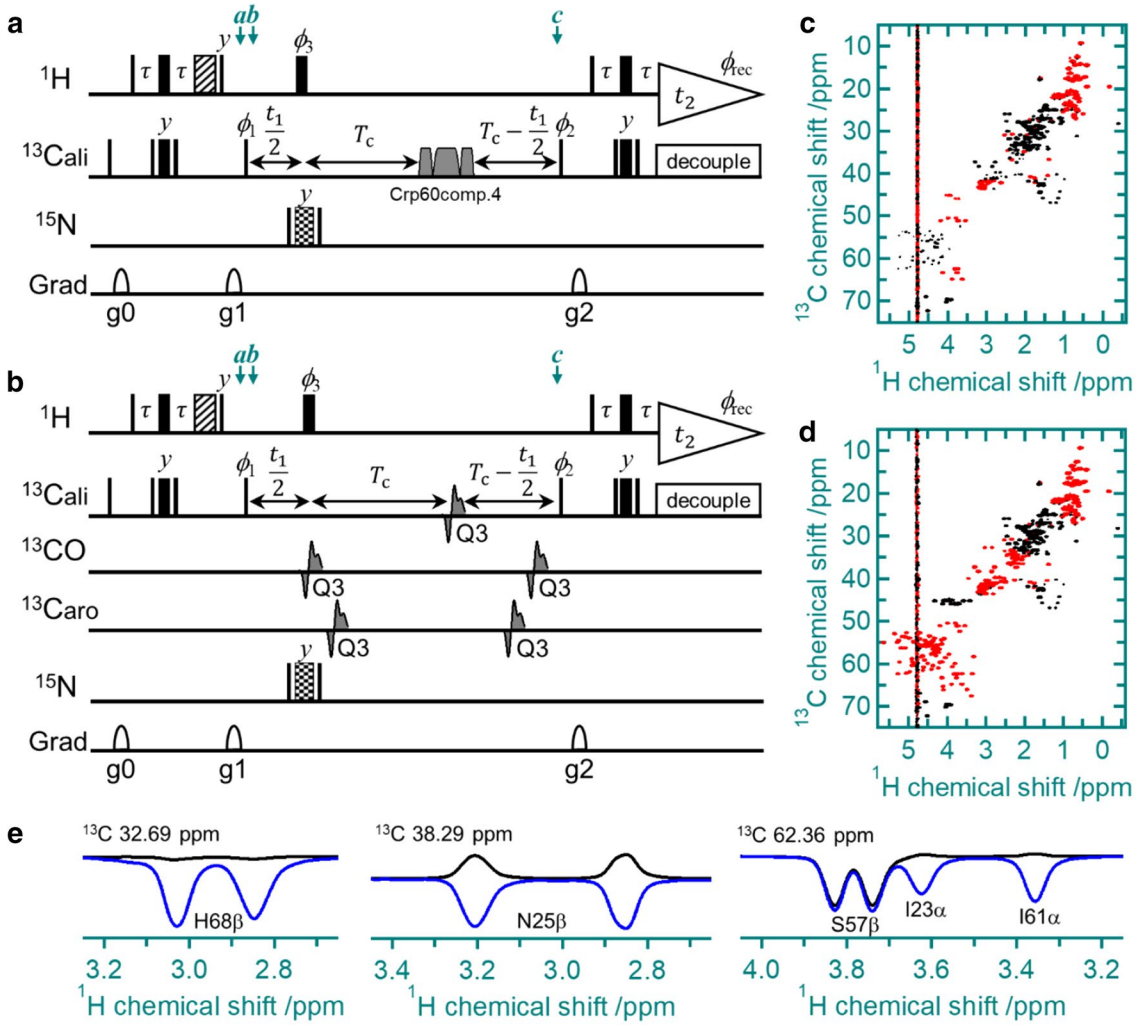

Fig. 1 Broadband and band-selective 2D CT ^{13}C–^{1}H HSQC experiments. **a** Pulse sequence of the 2D CT ^{13}C–^{1}H HSQC with an adiabatic pulse. A 2-ms composite smoothed Chirp (Crp60comp.4) (Hwang et al. 1997) centered at 100 ppm was used for refocusing of $^{13}C_{ali}$ transverse magnetization and for broadband inversion of longitudinal magnetization of the neighboring ^{13}C nuclei. **b** Pulse sequence of the 2D CT ^{13}C–^{1}H HSQC with band-selective ^{13}C pulses. For ^{13}C band-selective irradiations on the $^{13}C_{ali}$, ^{13}CO, and $^{13}C_{aro}$ regions with a flip angle of 180°, Q3 pulses (Emsley and Bodenhausen 1992) with durations of 375, 1020, and 510 µs, respectively, were used at the magnetic field of 11.7 T (i.e. ^{1}H frequency of 500 MHz). In the pulse sequences (panels a and b), the *narrow* and *wide* filled bars correspond to hard pulses with flip angles of 90° and 180°, respectively. All pulses were applied with phase x unless otherwise indicated. The hatched bar represents a trim pulse along the x-axis for a duration of 1 ms to suppress unwanted magnetization (Otting and Wüthrich 1988). Composite pulses on ^{13}C were used for the INEPT and reverse-INEPT steps (Levitt and Freeman 1979). For ^{13}C,^{15}N-labelled samples, a simultaneous inversion of the ^{15}N magnetization for lysine $^{15}N^{\zeta}$ and arginine $^{15}N^{\varepsilon}$ together with backbone ^{15}N nuclei can be effectively achieved by a composite pulse, 90°(x)-240°(y)-90°(x) (Freeman et al. 1980), with the ^{15}N frequency placed at 84 ppm. The pulsed field gradients along the z-axis, g0, g1, and g2, were 1 ms in length. The spectrum was collected with the following phase cycle: $\phi_1 = (x, -x)$, $\phi_2 = (x, x, -x, -x)$, $\phi_3 = (x, x, x, x, -x, -x, -x, -x)$, and $\phi_{rec} = (x, -x, -x, x)$. The delays were: $\tau = 1.7$ ms, $T_C = 14$ or 28 ms, The GARP decoupling scheme (Shaka et al. 1985) was applied with a radiofrequency field of 3.6 kHz during acquisition (t_2). Quadrature detection in the t_1 dimension was achieved with States-TPPI (Marion et al. 1989), where the phase ϕ_1 was increased by 90°. **c** 2D CT ^{13}C – ^{1}H HSQC spectrum of ^{13}C-enriched ubiquitin collected using the pulse sequence shown in panel a. **d** 2D CT ^{13}C–^{1}H HSQC spectrum of ^{13}C-enriched ubiquitin collected using the pulse sequence shown in panel b. **e** 1D slices of the 2D CT ^{13}C–^{1}H HSQC spectra of panels c (*black*) and d (*blue*). The side-chain $^1J_{CCaro}$ coupling of H68 and $^1J_{CCO}$ coupling of N25 are 54.7 and 49.3 Hz, respectively, and the backbone $^1J_{CCO}$ couplings of I23 and I61 are 54.2 Hz (Supplementary Tables S1 and S2)

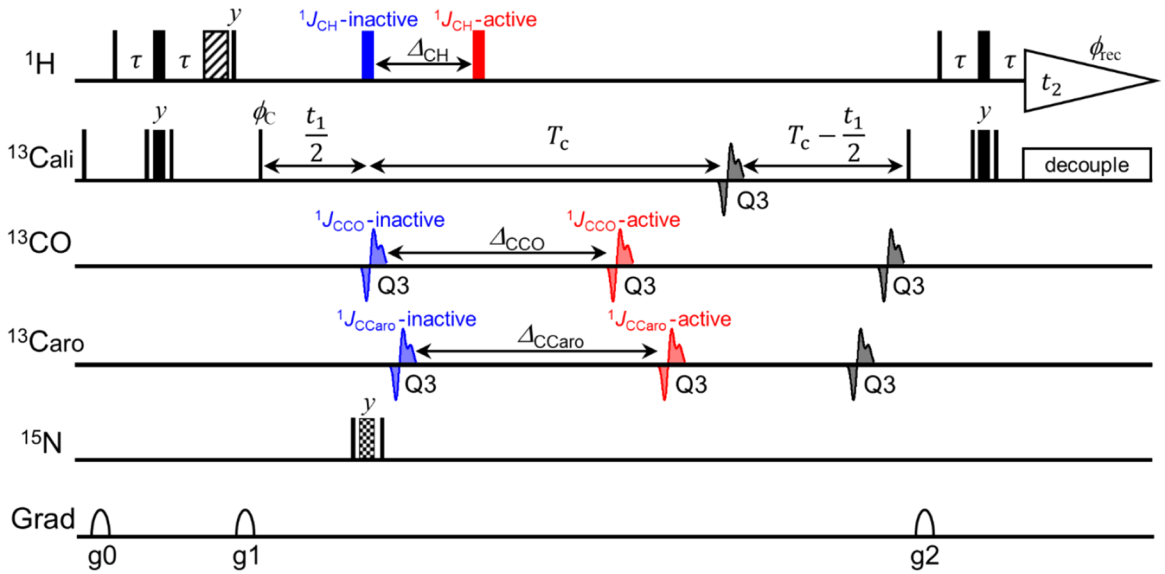

Fig. 2 Pulse sequence of the OROCHI experiment for recording eight binary combinations of 2D CT ^{13}C–^{1}H HSQC sub-spectra. For each of the $^{1}J_{CH}$, $^{1}J_{CCO}$, and $^{1}J_{CCaro}$ couplings, the pulses shown in *blue* were applied for the *J*-inactive experiments, whereas the pulses in *red* were for the *J*-active experiments. Unless otherwise indicated, the phases of ϕ_C and ϕ_{rec} are *x* when both $^{1}J_{CCO}$ and $^{1}J_{CCaro}$ are either active or inactive and $-x$ when only one of either $^{1}J_{CCO}$ or $^{1}J_{CCaro}$ is active (see Table 1). The delays were: $\tau = 1.7$ ms, $T_C = 14$ or 28 ms, $\Delta_{CH} = 3.8$ ms, $\Delta_{CCaro} = 11$ ms, and $\Delta_{CCO} = 10$ ms. Quadrature detection in the t_1 dimension was achieved with States-TPPI (Marion et al. 1989), where the phase ϕ_C was increased by 90°. All other parameters are the same as in Fig. 1. The pulse sequence code for Bruker spectrometers is provided in the Supplementary Material. In the pulse sequence, the use of solvent presaturation during the recycle delay is optional

$$\begin{bmatrix} S_1 \\ \vdots \\ S_N \end{bmatrix} = H_N \begin{bmatrix} s_1 \\ \vdots \\ s_N \end{bmatrix} \tag{1a}$$

where H_N, a Hadamard matrix of order N, is given by the following recursive definition with $H_1 = 1$:

$$H_{2^k} = \begin{bmatrix} H_{2^{k-1}} & H_{2^{k-1}} \\ H_{2^{k-1}} & -H_{2^{k-1}} \end{bmatrix} \tag{1b}$$

where k is a positive integer. NMRPipe scripts are provided in the Supplementary Material for generating separate time-domain FID data according to Hadamard transform of the interleaved raw FID before processing so that mirror-image linear prediction (LP) in the ^{13}C dimension can be separately applied to the spectra. This is advantageous as these are more sparse and the reduced number of signals improves the robustness of root finding by the LP algorithm. These separate FIDs are apodized with a squared cosine function before zero filling and Fourier transform in both ^{1}H and ^{13}C dimensions.

Results and discussion

Figure 3 shows separation of NMR signals of ubiquitin by means of individual sign-encoding with $^{1}J_{CH}$, $^{1}J_{CCO}$, and $^{1}J_{CCaro}$ couplings. The *J*-coupling evolution is inactive in one of the two sub-spectra (Fig. 3a) and is active in the other (Fig. 3b–d). The resulting sum (S_{sum}) and difference (S_{dif}) spectra were obtained by the following equation:

$$\begin{bmatrix} S_{sum} \\ S_{dif} \end{bmatrix} = H_2 \begin{bmatrix} s_{inactive} \\ s_{active} \end{bmatrix} \tag{2a}$$

where $s_{inactive}$ and s_{active} are the *J*-inactive and *J*-active sub-spectra, respectively. H_2 is a Hadamard matrix of order 2 (H_2):

$$H_2 = \begin{bmatrix} 1 & 1 \\ 1 & -1 \end{bmatrix} \tag{2b}$$

As shown in Fig. 3e,h, the sum and difference of the $^{1}J_{CH}$-inactive and $^{1}J_{CH}$-active sub-spectra at a ratio of one to one

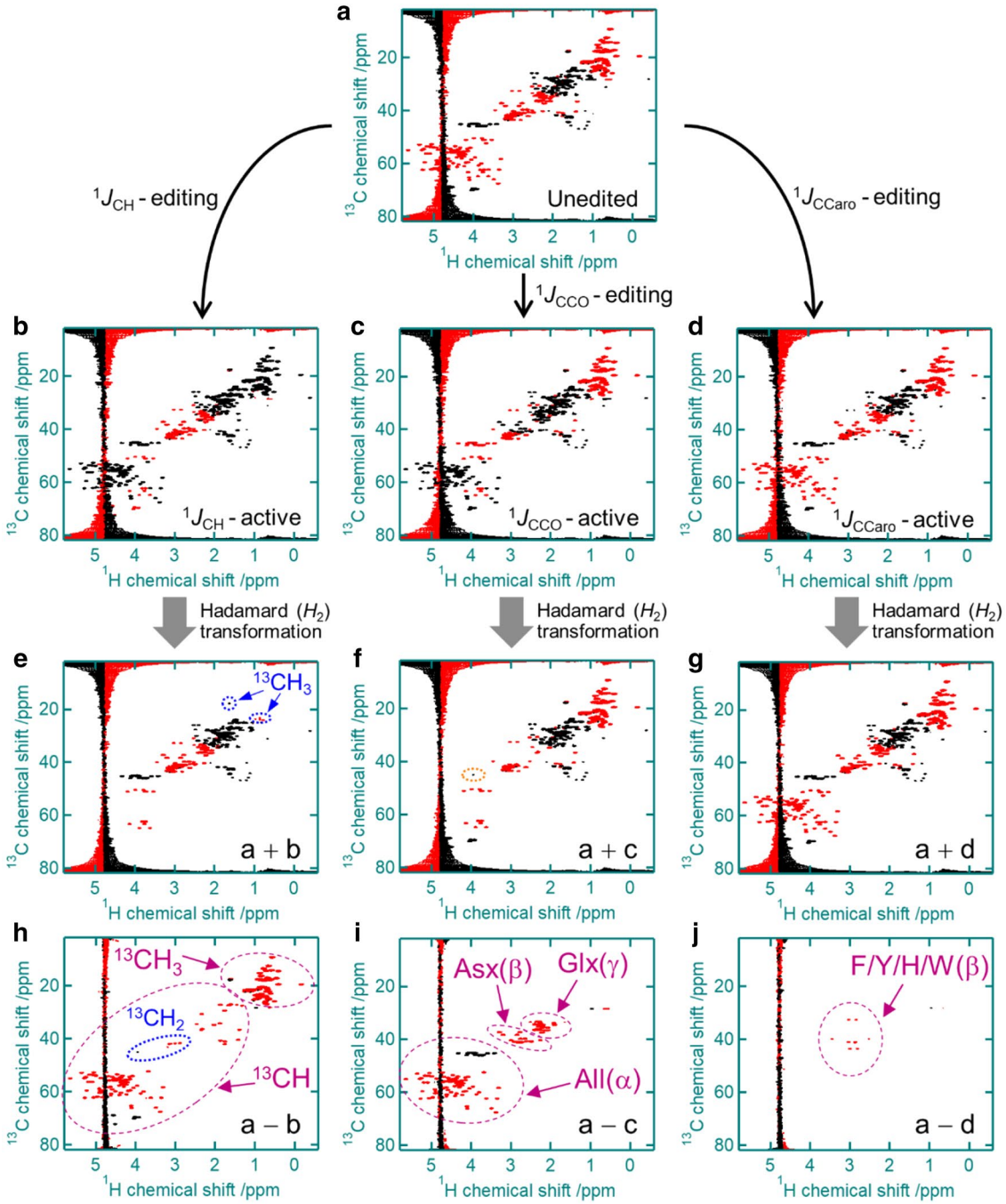

Fig. 3 **a–d** 2D CT ^{13}C–^{1}H HSQC sub-spectra of ^{13}C-enriched ubiquitin collected using the pulse sequence shown in Fig. 2, where the phases of ϕ_C and ϕ_{rec} were kept *x*. The CT period ($2Tc$) was set at 28 ms. The *positive* and *negative* peaks are shown in *black* and *red*, respectively. **a** Unedited (i.e. $^{1}J_{CH}$-inactive, $^{1}J_{CCO}$-inactive, and $^{1}J_{CCaro}$-inactive) sub-spectrum. **b** $^{1}J_{CH}$-active sub-spectrum. The $^{1}J_{CCO}$- and $^{1}J_{CCaro}$-editings were inactive. **c** $^{1}J_{CCO}$-active sub-spectrum. The $^{1}J_{CH}$- and $^{1}J_{CCaro}$-editings were inactive. **d** $^{1}J_{CCaro}$-active sub-spectrum. The $^{1}J_{CH}$- and $^{1}J_{CCO}$-editings were inactive. **e–j** Linear combination of the sum (e–g) and difference (h–j) of the 2D CT ^{13}C–^{1}H HSQC sub-spectra. In panels e and h, undesired artifacts due to $^{1}J_{CH}$ mismatch are indicated in *blue* dotted circles. In panel f, $^{1}J_{CCO}$-mismatched artifact is indicated in an *orange* dotted circle

therefore yielded the $^{13}CH_2$ and the $^{13}CH/^{13}CH_3$ spectra. In the same way, subtraction of the $^{1}J_{CCO}$-inactive and $^{1}J_{CCO}$-active sub-spectra separated the Asx $^{13}C^{\beta}$–$^{1}H^{\beta}$ and Glx $^{13}C^{\gamma}$–$^{1}H^{\gamma}$ correlations together with $^{13}C^{\alpha}$–$^{1}H^{\alpha}$ of all residues (Fig. 3f,i). Likewise, the difference spectrum calculated from the $^{1}J_{CCaro}$-inactive and $^{1}J_{CCaro}$-active sub-spectra selected

the $^{13}C^{\beta}-^{1}H^{\beta}$ resonances of aromatic amino acid residues (Fig. 3g,j). As individual sub-spectra shown in Fig. 3a–d were obtained in a single scan per indirect increment, the undesired magnetization from residual water, which is not scalar-coupled to ^{13}C, at the point of acquisition gave rise to spectral artifact in the sum spectra (Fig. 3e–g) whereas it was effectively suppressed in the difference spectra which were generated by subtraction between the two sub-spectra (Fig. 3h–j). While repetition of the experiment with a phase cycling scheme can eliminate the solvent artifact, we will, instead of increasing the number of scans, introduce a combinational sign-encoding strategy with $^{1}J_{CH}$, $^{1}J_{CCO}$, and $^{1}J_{CCaro}$ couplings, where eight sub-spectra are recorded in a single scan per indirect increment.

In the OROCHI experiment, eight combinations of multiplicity-edited 2D CT $^{13}C-^{1}H$ HSQC sub-spectra with three binary parameters (i.e., whether each of the $^{1}J_{CH}$-, $^{1}J_{CCO}$-, and $^{1}J_{CCaro}$-coupling evolution periods was included or removed) were recorded. Linear combinations of sums and differences of these eight sub-spectra (s_1 to s_8) generated a series of multiplicity-separated NMR spectra (S_1 to S_8):

$$S = H_8 S_{sub} \tag{3a}$$

where S and S_{sub} are the column vector represented respectively by $S=[S_1\ S_2\ S_3\ \ldots\ S_8]^T$ and $S_{sub}=[s_1\ s_2\ s_3\ \ldots\ s_8]^T$. H_8 is a Hadamard matrix of order 8, that is,

$$H_8 = \begin{bmatrix} 1 & 1 & 1 & 1 & 1 & 1 & 1 & 1 \\ 1 & -1 & 1 & -1 & 1 & -1 & 1 & -1 \\ 1 & 1 & -1 & -1 & 1 & 1 & -1 & -1 \\ 1 & -1 & -1 & 1 & 1 & -1 & -1 & 1 \\ 1 & 1 & 1 & 1 & -1 & -1 & -1 & -1 \\ 1 & -1 & 1 & -1 & -1 & 1 & -1 & 1 \\ 1 & 1 & -1 & -1 & -1 & -1 & 1 & 1 \\ 1 & -1 & -1 & 1 & -1 & 1 & 1 & -1 \end{bmatrix} \tag{3b}$$

Listed in Table 1 are the eight binary combinations of the 2D CT $^{13}C-^{1}H$ HSQC sub-spectra. As shown in Table 2, Hadamard transform of these sub-spectra generates five HSQC spectra (S_1 to S_5) with desired signals, while the last three (S_6, S_7, and S_8) are empty. When the phases of the ^{13}C excitation pulse (ϕ_C) and the receiver (ϕ_{rec}) were fixed for all sub-spectra in the OROCHI experiment, the solvent artifact appeared in the spectrum S_1, which was generated by adding up the eight sub-spectra (Supplementary Fig. S2). To avoid the risk of peak burial in the solvent artifact, the solvent artifact can be moved to an empty spectrum. In Supplementary Fig. S3, the phases of ϕ_C and ϕ_{rec} were x when both $^{1}J_{CCO}$ and $^{1}J_{CCaro}$ were either active or inactive and $-x$ when only one of either $^{1}J_{CCO}$ or $^{1}J_{CCaro}$ was active (see Table 1), so that the solvent artifact accumulated in the S_7 spectrum. We note that the solvent resonance in each HSQC spectrum could further be suppressed by presaturation although irradiation of $^{1}H^{\alpha}$ resonances that are close to the solvent frequency would result in their absence from the spectrum.

Figure 4 shows separation of NMR signals of ubiquitin by means of combinatorial sign-encoding with $^{1}J_{CH}$, $^{1}J_{CCO}$, and $^{1}J_{CCaro}$ couplings. The S_5 spectrum selected $^{13}C_{aro}$-coupled $^{13}CH_2$ correlations, that is, F/Y/H/W $^{13}C^{\beta}-^{1}H^{\beta}$ correlations.

Table 1 Eight combinations of 2D CT $^{13}C-^{1}H$ HSQC sub-spectra (s_1 to s_8)

	$^{1}J_{CH}$ [a]	$^{1}J_{CCO}$ [a]	$^{1}J_{CCaro}$ [a]	ϕ_C	ϕ_{rec}
s_1	−	−	−	$+x$	$+x$
s_2	+	−	−	$+x$	$+x$
s_3	−	+	−	$-x$	$-x$
s_4	+	+	−	$-x$	$-x$
s_5	−	−	+	$-x$	$-x$
s_6	+	−	+	$-x$	$-x$
s_7	−	+	+	$+x$	$+x$
s_8	+	+	+	$+x$	$+x$

[a]The *J*-active and *J*-inactive experiments are represented by the symbols + and −, respectively

Table 2 All possible linear combinations of sums and differences of the *J*-active and *J*-inactive sub-spectra according to the Hadamard transform

	s_1	s_2	s_3	s_4	s_5	s_6	s_7	s_8	Selected resonances		
									$^{13}CH_2$ or $^{13}CH/^{13}CH_3$	Coupled to ^{13}CO	Coupled to $^{13}C_{aro}$
S_1	+	+	+	+	+	+	+	+	$^{13}CH_2$	No	No
S_2	+	−	+	−	+	−	+	−	$^{13}CH/^{13}CH_3$	No	No
S_3	+	+	−	−	+	+	−	−	$^{13}CH_2$	Yes	No
S_4	+	−	−	+	+	−	−	+	$^{13}CH/^{13}CH_3$	Yes	No
S_5	+	+	+	+	−	−	−	−	$^{13}CH_2$	No	Yes
S_6	+	−	+	−	−	+	−	+	$^{13}CH/^{13}CH_3$	No	Yes
S_7	+	+	−	−	−	−	+	+	$^{13}CH_2$	Yes	Yes
S_8	+	−	−	+	−	+	+	−	$^{13}CH/^{13}CH_3$	Yes	Yes

The last three spectra (S_6, S_7, and S_8) are empty (see Supplementary Figs. S2 and S3)

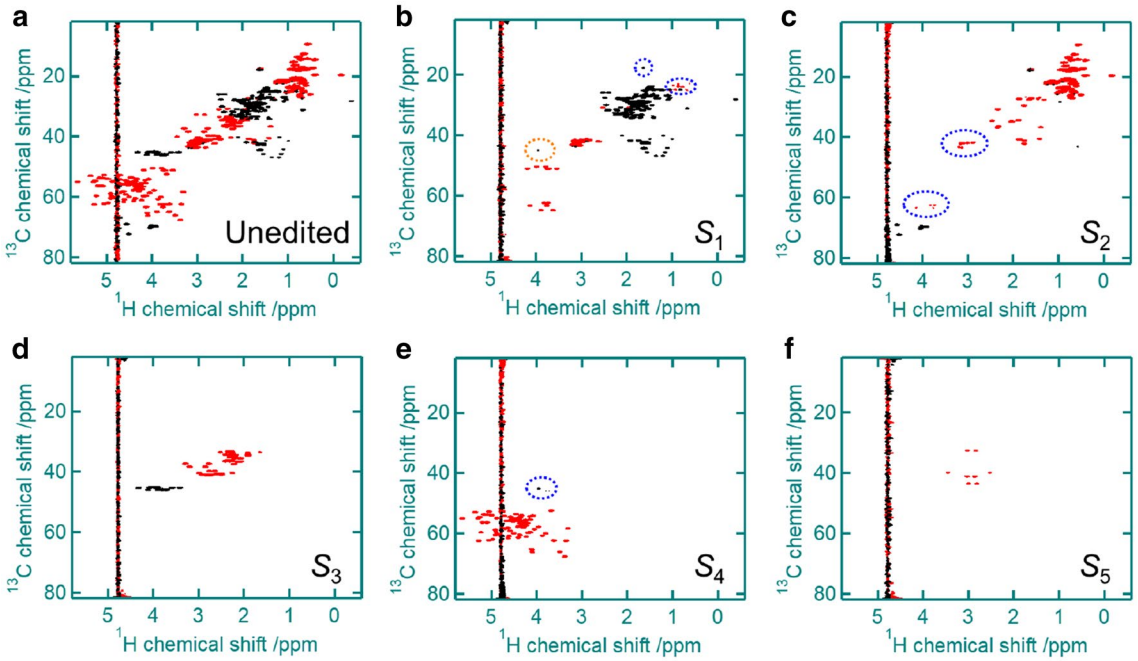

Fig. 4 Selective observation of complementary NMR signals with an OROCHI experiment on ^{13}C-enriched ubiquitin. In the 2D CT ^{13}C–^{1}H HSQC experiments, the CT period ($2Tc$) was set at 28 ms. The *positive* and *negative* peaks are shown in *black* and *red*, respectively. **a** Unedited 2D CT ^{13}C–^{1}H HSQC spectrum (same as Fig. 1d). **b–f** Multiplicity-separated 2D CT ^{13}C–^{1}H HSQC spectra generated by linear combinations of the sums and differences of the sub-spectra with the Hadamard matrix of order 8. A series of 2D CT ^{13}C–^{1}H HSQC sub-spectra, shown in Supplementary Fig. S3a, were collected using the pulse sequence shown in Fig. 2. Undesired artifacts due to $^{1}J_{CH}$ mismatch are indicated in *blue* dotted circles, and $^{1}J_{CCO}$-mismatched artifact is indicated in an *orange* dotted circle. All the eight spectra (S_1 to S_8) are shown in Supplementary Fig. S3b

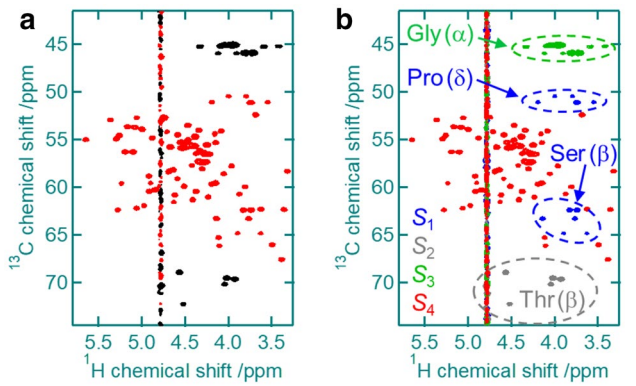

Fig. 5 Distinguishing side-chain $^{13}CH_2$ groups from backbone $^{13}C^{\alpha}$–$^{1}H^{\alpha}$ correlations. In the 2D ^{13}C–^{1}H HSQC experiment, the CT period ($2Tc$) was set at 28 ms. **a** Unedited spectrum of ^{13}C-enriched ubiquitin. The *positive* and *negative* peaks are shown in *black* and *red*, respectively. **b** Corresponding multiplicity-separated spectrum of ^{13}C-enriched ubiquitin. The S_1, S_2, S_3, and S_4 spectra are color-coded in *blue*, *gray*, *green*, and *red*, respectively, and superimposed on the same spectrum

The S_4 spectrum was for ^{13}CO-coupled $^{13}CH/^{13}CH_3$ groups; it selected $^{13}C^{\alpha}$–$^{1}H^{\alpha}$ correlations of all residues but glycine. In the S_3 spectrum, the Asx $^{13}C^{\beta}$–$^{1}H^{\beta}$ and Glx $^{13}C^{\gamma}$–$^{1}H^{\gamma}$ correlations together with $^{13}C^{\alpha}$–$^{1}H^{\alpha}$ of glycine residues were obtained. Other aliphatic $^{13}CH/^{13}CH_3$ and $^{13}CH_2$ groups were separated in the S_2 and S_1 spectra, respectively. It is possible to further enhance the resolution in the ^{13}C dimension by extending the CT period, $2T_C$, from $1/^{1}J_{CC}$ (~28 ms) to $2/^{1}J_{CC}$ (~56 ms) unless the attenuation of the signals during the CT period due to ^{13}C transverse relaxation is prohibitive (Supplementary Fig. S4). On the other hand, signals displayed with opposite sign can be distinguished when $2T_C = 1/^{1}J_{CC}$. For example, methionine γ-$^{13}CH_2$ and ε-$^{13}CH_3$ correlations can be distinguished in the S_1 and S_2 spectra, respectively. Figure 5 shows an expanded region of the 2D CT ^{13}C–^{1}H HSQC to display backbone $^{13}C^{\alpha}$–$^{1}H^{\alpha}$ correlations. In the unedited spectrum, serine β-$^{13}CH_2$ and proline δ-$^{13}CH_2$ correlations were indistinguishable (Fig. 5a). In contrast, these correlations were readily separated in the OROCHI experiment (Fig. 5b). Separation of aliphatic NMR signals in the OROCHI experiment is summarized in Table 3.

Figure 6 shows an expanded region of the 2D CT ^{13}C–^{1}H HSQC of ubiquitin. In the unedited spectrum, the left-side peak of the F45 $^{13}C^{\beta}$–$^{1}H^{\beta}$ correlations was hidden under the intense peak due to R42 δ-$^{13}CH_2$. In addition, the right-side peak of the F4 $^{13}C^{\beta}$–$^{1}H^{\beta}$ correlations overlapped with

Table 3 Separation of aliphatic NMR signals in the OROCHI experiment

Amino acid	Atom name	Number of adjacent nuclei					Spectrum	Signal phase [a]
		^{1}H	^{13}CO	$^{13}C_{aro}$	$^{13}C_{ali}$	Others		
All amino acids except glycine	CA	2	1	0	0	1	S_4	Negative
G	CA	2	1	0	0	1	S_3	Positive
A	CB	3	0	0	1	0	S_2	Negative
V	CB	1	0	0	3	0	S_2	Negative
	CG1/CG2	3	0	0	1	0	S_2	Negative
L	CB	2	0	0	2	0	S_1	Positive
	CG	1	0	0	3	0	S_2	Negative
	CD1/CD2	3	0	0	1	0	S_2	Negative
I	CB	1	0	0	3	0	S_2	Negative
	CG1	2	0	0	2	0	S_1	Positive
	CG2/CD1	3	0	0	1	0	S_2	Negative
P/R	CB/CG	2	0	0	2	0	S_1	Positive
	CD	2	0	0	1	1	S_1	Negative
K	CB/CG/CD	2	0	0	2	0	S_1	Positive
	CE	2	0	0	1	1	S_1	Negative
D/N	CB	2	1	0	1	0	S_3	Negative
E/Q	CB	2	0	0	2	0	S_1	Positive
	CG	2	1	0	1	0	S_3	Negative
F/Y/H/W	CB	2	0	1	1	0	S_5	Negative
M	CB	2	0	0	2	0	S_1	Positive
	CG	2	0	0	1	1	S_1	Negative
	CE	3	0	0	0	1	S_2	Positive
C/S	CB	2	0	0	1	1	S_1	Negative
T	CB	1	0	0	2	1	S_2	Positive
	CG2	3	0	0	1	0	S_2	Negative

[a]When the CT period ($2T_C$) is set at $2/^{1}J_{CC}$ (~56 ms), all signals have the same sign

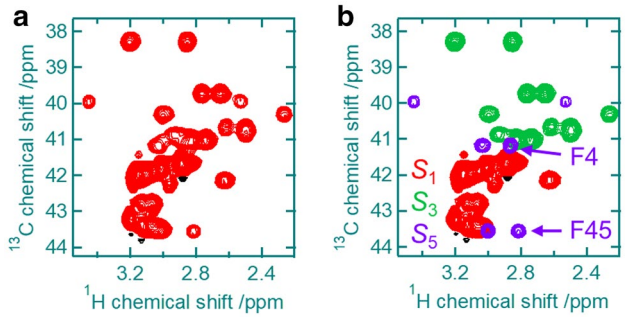

Fig. 6 Resolving resonance overlap in the 2D $^{13}C-^{1}H$ HSQC spectrum of ^{13}C-enriched ubiquitin. The CT period ($2Tc$) was set at 28 ms. **a** A close-up view of the unedited spectrum. **b** Corresponding multiplicity-separated spectrum. The S_1, S_3, and S_5 spectra are color-coded in *red*, *green*, and *purple*, respectively, and superimposed on the same spectrum. Each of these spectra are shown in Supplementary Fig. S5

a β-$^{13}CH_2$ correlation due to D32. In the multiplicity-separated spectra, on the other hand, the F45 and F4 $^{13}C^{\beta}-^{1}H^{\beta}$ correlations obtained by the OROCHI experiment were resolved unambiguously (see Fig. 6 and Supplementary Fig. S5). Although NMR experiments can allow elimination of resonance overlap by introducing additional spectral dimensions (Supplementary Fig. S5d), these experiments require longer measurement time. In addition, working with 2D data is more intuitive and data manipulations are easy (Walinda et al. 2017). Such simplified HSQC experiments can greatly facilitate NMR titration experiments with ligand or pH, where spectral crowding is often a limiting factor. The ability to generate 2D $^{13}C-^{1}H$ maps may be particularly fruitful for the characterization of protein–protein and protein–ligand interactions, as the ^{13}C and ^{1}H chemical shift changes of aliphatic groups due to binding may be understood in structural terms more readily than those of backbone amide ^{15}N and ^{1}H groups (Williamson 2013).

As a drawback, we acknowledge that, while no additional relaxation loss was generated by the sign-encoding strategy achieved within the CT ^{13}C chemical shift evolution period, deviation of the J coupling from the nominal value can lead to sensitivity losses and the appearance of spectral artifacts (Figs. 3 and 4 and Supplementary Figs. S2 and S3). Aliphatic $^{1}J_{CH}$ couplings range from 125 to 160 Hz (Zwahlen et al. 1997). For example, the $^{1}J_{CH}$ coupling for the M1 ε-$^{13}CH_3$ group of ubiquitin was 142 Hz, while the average $^{1}J_{CH}$ coupling for leucine δ-$^{13}CH_3$ groups

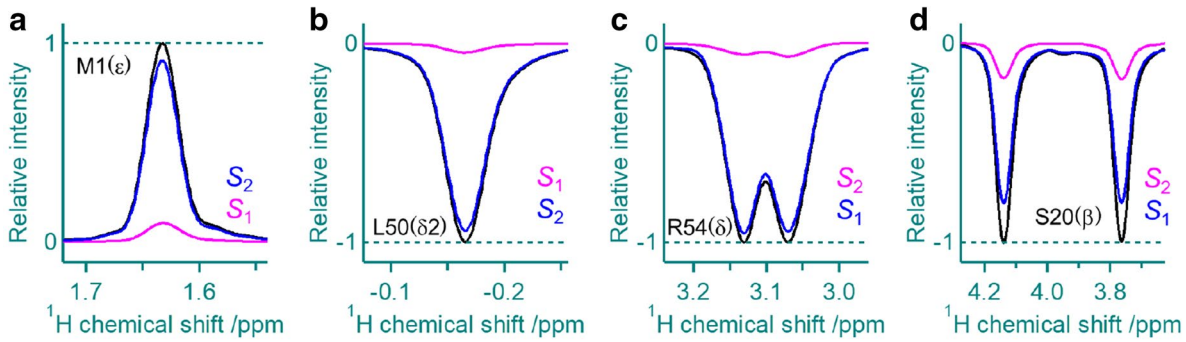

Fig. 7 Imperfect cancellation due to mismatch of $^{1}J_{CH}$ couplings. Shown are 1D slices for the M1 ε-$^{13}CH_3$ (**a**), L50 δ2-$^{13}CH_3$ (**b**), R54 δ-$^{13}CH_2$ (**c**), and S20 β-$^{13}CH_2$ (**d**) correlations. The CT period ($2T_C$) was set at 28 ms. Unedited and multiplicity-separated spectra are indicated in *black* and *blue*, respectively. The corresponding spectra with *J*-mismatched artifacts are shown in *magenta*

was 125 Hz (Supplementary Fig. S6a, b). In the $^{1}J_{CH}$-active experiment, the net $^{1}J_{CH}$-evolution time ($2\Delta_{CH}$) was set so that a compromise of $^{1}J_{CH}=130$ Hz was used. As shown in Fig. 7, the ratio of the signal intensity in the S_2 spectrum to that of the corresponding unedited spectrum was 91% for M1 ε-$^{13}CH_3$ and 94% for L50 δ2-$^{13}CH_3$. Imperfect cancellation for intense $^{13}CH_3$ peaks resulted in detectable artifacts in the methyl region of the added spectrum that selected aliphatic $^{13}CH_2$ groups (Supplementary Fig. S7). On the other hand, for intense signals of $^{13}CH_2$ groups (e.g. arginine δ-$^{13}CH_2$, lysine ε-$^{13}CH_2$, and serine β-$^{13}CH_2$), imbalance due to $^{1}J_{CH}$ mismatch caused artifacts that appeared with attenuated intensity. The average $^{1}J_{CH}$ couplings are 146, 145, and 156 Hz for arginine δ-$^{13}CH_2$, lysine ε-$^{13}CH_2$, and serine β-$^{13}CH_2$ groups, respectively (Supplementary Fig. S6c, d). The average drop in the intensity was 10% for lysine ε-$^{13}CH_2$, 5% for arginine δ-$^{13}CH_2$ and 17% for serine β-$^{13}CH_2$ (Fig. 7 and Supplementary Fig. S8). The $^{1}J_{CCO}$ and $^{1}J_{CCaro}$ couplings were obtained from peak splitting along the ^{13}C dimension of a 2D CT $^{13}C-^{1}H$ HSQC spectrum without pulses on ^{13}CO and $^{13}C_{aro}$ carbons (Supplementary Fig. S9). For well-resolved resonances, the $^{1}J_{CCO}$ and $^{1}J_{CCaro}$ coupling values were obtained (Supplementary Tables S1 and S2). The average $^{1}J_{CCO}$ and $^{1}J_{CCaro}$ couplings are 52.2 and 46.1 Hz, respectively. In the OROCHI experiments, we used the $^{1}J_{CCO}$ and $^{1}J_{CCaro}$ values of 50 and 45 Hz, respectively. Mismatch of the $^{1}J_{CCO}$ and $^{1}J_{CH}$ couplings of intense glycine α-$^{13}CH_2$ correlations resulted in appearance of the mismatched artifact in the S_1 and S_4 spectra (Fig. 4 and Supplementary Fig. S10). Mismatch of the $^{1}J_{CCaro}$ coupling was seen for H68 β-$^{13}CH_2$ (Supplementary Fig. S11).

It has been pointed out that strong couplings that occur when the chemical shift difference between the two coupling ^{13}C nuclei is not sufficiently larger than $^{1}J_{CC}$ could cause serious distortion of the spectrum (Vuister and Bax 1992). In the case of limited leucine side-chain mobility in proteins, one of the methyl groups may have the $^{13}C^{\delta}$ frequency close to the chemical shift of the neighboring $^{13}C^{\gamma}$ nuclei (Mulder 2009; Hoffmann et al. 2018). There are a few more residues where the chemical shifts of the neighbors can be close to each other: serine $^{13}C^{\alpha}/^{13}C^{\beta}$, arginine $^{13}C^{\beta}/^{13}C^{\gamma}$, and methionine $^{13}C^{\beta}/^{13}C^{\gamma}$. Nevertheless, the artifact caused by strong couplings is not usually a significant issue in the aliphatic $^{13}C-^{1}H$ HSQC experiments (Vuister and Bax 1992).

In conclusion, we have introduced OROCHI, a method for selective observation of complementary NMR signals by combinatorial editing of 2D CT $^{13}C-^{1}H$ HSQC spectroscopy using $^{1}J_{CCaro}$, $^{1}J_{CCO}$, and $^{1}J_{CH}$ couplings. ^{13}CO-coupled side-chain $^{13}CH_2$ correlations of Asx/Glx residues and $^{13}C_{aro}$-coupled β-$^{13}CH_2$ correlations of aromatic amino acid residues are easily separated in the S_3 and S_5 spectra, respectively. Spectral simplification alleviates resonance overlap and can be useful for unambiguous resonance assignment. It may also be possible to separate tryptophan from the other three aromatic amino acid residues (i.e. phenylalanine, tyrosine, and histidine) if the selective pulses are finely tuned (Schubert et al. 2001b). In addition, OROCHI may benefit from methods for improved suppression of $^{1}J_{CH}$-dependent artifacts (Zwahlen et al. 1997; Brutscher 2001; Boyer et al. 2003; Heikkinen et al. 2003), albeit at the expense of lengthening experimental time. The demonstrated method would provide a basis of multi-dimensional NMR experiments with $^{13}C_{ali}$ frequency encoding in a CT chemical shift evolution manner, so long as signal attenuation due to ^{13}C transverse relaxation is acceptable.

Acknowledgements This work was performed under the Cooperative Research Programs at the Institute for Protein Research, Osaka University (NMRCR-17-05 and NMRCR-18-05). We thank Dr. Yohei Miyanoiri (Institute for Protein Research, Osaka University) for help with NMR analysis. This work was supported by JSPS KAKENHI (Grant Number JP 19K14677) and the Uehara Memorial Foundation.

References

Bax A, Ikura M, Kay LE, Torchia DA, Tschudin R (1990) Comparison of different modes of two-dimensional reverse-correlation NMR for the study of proteins. J Magn Reson 86:304–318. https://doi.org/10.1016/0022-2364(90)90262-8

Bendall MR, Doddrell DM, Pegg DT (1981) Editing of carbon-13 NMR spectra. 1. A pulse sequence for the generation of subspectra. J Am Chem Soc 103:4603–4605. https://doi.org/10.1021/ja00405a062

Bodenhausen G, Ruben DJ (1980) Natural abundance nitrogen-15 NMR by enhanced heteronuclear spectroscopy. Chem Phys Lett 69:185–189. https://doi.org/10.1016/0009-2614(80)80041-8

Boyer RD, Johnson R, Krishnamurthy K (2003) Compensation of refocusing inefficiency with synchronized inversion sweep (CRISIS) in multiplicity-edited HSQC. J Magn Reson 165:253–259. https://doi.org/10.1016/j.jmr.2003.08.009

Brenner AK, Frøystein NÅ (2014) Using MUSIC and CC(CO)NH for backbone assignment of two medium-sized proteins not fully accessible to standard 3D NMR. Molecules 19:8890–8903. https://doi.org/10.3390/molecules19078890

Brutscher B (2001) Accurate measurement of small spin-spin couplings in partially aligned molecules using a novel J-mismatch compensated spin-state-selection filter. J Magn Reson 151:332–338. https://doi.org/10.1006/jmre.2001.2375

Brutscher B (2004) Combined frequency- and time-domain NMR spectroscopy. Application to fast protein resonance assignment. J Biomol NMR 29:57–64. https://doi.org/10.1023/B:JNMR.0000019501.21697.34

Bystrov VF (1976) Spin-spin coupling and the conformational states of peptide systems. Prog Nucl Magn Reson Spectrosc 10:41–82. https://doi.org/10.1016/0079-6565(76)80001-5

Chen K, Freedberg DI, Keire DA (2015) NMR profiling of biomolecules at natural abundance using 2D ^{1}H–^{15}N and ^{1}H–^{13}C multiplicity-*separated* (MS) HSQC spectra. J Magn Reson 251:65–70. https://doi.org/10.1016/j.jmr.2014.11.011

Davis DG (1990) Simplification of proton-detected, natural abundance carbon-13 correlation spectra of proteins via multiplet editing. J Magn Reson 90:589–596. https://doi.org/10.1016/0022-2364(90)90067-J

Davis DG (1991) Improved multiplet editing of proton-detected, heteronuclear shift-correlation spectra. J Magn Reson 91:665–672. https://doi.org/10.1016/0022-2364(91)90398-D

Delaglio F, Grzesiek S, Vuister GW, Zhu G, Pfeifer J, Bax A (1995) NMRPipe: a multidimensional spectral processing system based on UNIX pipes. J Biomol NMR 6:277–293. https://doi.org/10.1007/BF00197809

Doddrell DM, Pegg DT, Bendall MR (1982) Distortionless enhancement of NMR signals by polarization transfer. J Magn Reson 48:323–327. https://doi.org/10.1016/0022-2364(82)90286-4

Dubey A, Mondal S, Chandra K, Atreya HS (2016) Rapid identification of amino acid types in proteins using phase modulated 2D HN(CACB) and 2D HN(COCACB). J Magn Reson 267:22–29. https://doi.org/10.1016/j.jmr.2016.04.004

Emsley L, Bodenhausen G (1992) Optimization of shaped selective pulses for NMR using a quaternion description of their overall propagators. J Magn Reson 97:135–148. https://doi.org/10.1016/0022-2364(92)90242-Y

Feng W, Rios CB, Montelione GT (1996) Phase labeling of C-H and C-C spin-system topologies: application in PFG-HACANH and PFG-HACA(CO)NH triple-resonance experiments for determining backbone resonance assignments in proteins. J Biomol NMR 8:98–104. https://doi.org/10.1007/BF00198144

Feuerstein S, Plevin MJ, Willbold D, Brutscher B (2012) iHADAMAC: a complementary tool for sequential resonance assignment of globular and highly disordered proteins. J Magn Reson 214:329–334. https://doi.org/10.1016/j.jmr.2011.10.019

Freeman R, Kempsell SP, Levitt MH (1980) Radiofrequency pulse sequences which compensate their own imperfections. J Magn Reson 38:453–479. https://doi.org/10.1016/0022-2364(80)90327-3

Grzesiek S, Bax A (1993) Amino acid type determination in the sequential assignment procedure of uniformly ^{13}C/^{15}N-enriched proteins. J Biomol NMR 3:185–204. https://doi.org/10.1007/BF00178261

Heikkinen S, Toikka MM, Karhunen PT, Kilpeläinen IA (2003) Quantitative 2D HSQC (Q-HSQC) via suppression of *J*-dependence of polarization transfer in NMR spectroscopy: application to wood lignin. J Am Chem Soc 125:4362–4367. https://doi.org/10.1021/ja029035k

Hoffmann F, Xue M, Schafer LV, Mulder FAA (2018) Narrowing the gap between experimental and computational determination of methyl group dynamics in proteins. Phys Chem Chem Phys 20:24577–24590. https://doi.org/10.1039/C8CP03915A

Hwang T-L, van Zijl PCM, Garwood M (1997) Broadband adiabatic refocusing without phase distortion. J Magn Reson 124:250–254. https://doi.org/10.1006/jmre.1996.1049

Kay LE, Bax A (1989) Separation of NH and NH_2 resonances in ^{1}H-detected heteronuclear multiple-quantum correlation spectra. J Magn Reson 84:598–603. https://doi.org/10.1016/0022-2364(89)90125-X

Kessler H, Schmieder P, Kurz M (1989) Implementation of the DEPT sequence in inverse shift correlation; the DEPT-HMQC. J Magn Reson 85:400–405. https://doi.org/10.1016/0022-2364(89)90153-4

Kupče E, Nishida T, Freeman R (2003) Hadamard NMR spectroscopy. Prog Nucl Magn Reson Spectrosc 42:95–122. https://doi.org/10.1016/S0079-6565(03)00022-0

Lescop E, Rasia R, Brutscher B (2008) Hadamard amino-acid-type edited NMR experiment for fast protein resonance assignment. J Am Chem Soc 130:5014–5015. https://doi.org/10.1021/ja800914h

Levitt MH, Freeman R (1979) NMR population inversion using a composite pulse. J Magn Reson 33:473–476. https://doi.org/10.1016/0022-2364(79)90265-8

Marion D, Ikura M, Tschudin R, Bax A (1989) Rapid recording of 2D NMR spectra without phase cycling. Application to the study of hydrogen exchange in proteins. J Magn Reson 85:393–399. https://doi.org/10.1016/0022-2364(89)90152-2

Markley JL, Bax A, Arata Y, Hilbers CW, Kaptein R, Sykes BD, Wright PE, Wüthrich K (1998) Recommendations for the presentation of NMR structures of proteins and nucleic acids. IUPAC-IUBMB-IUPAB inter-union task group on the standardization of data bases of protein and nucleic acid structures determined by NMR spectroscopy. J Biomol NMR 12:1–23. https://doi.org/10.1023/a:1008290618449

Morris GA, Freeman R (1979) Enhancement of nuclear magnetic resonance signals by polarization transfer. J Am Chem Soc 101:760–762. https://doi.org/10.1021/ja00497a058

Mulder FAA (2009) Leucine side-chain conformation and dynamics in proteins from ^{13}C NMR chemical shifts. ChemBioChem 10:1477–1479. https://doi.org/10.1002/cbic.200900086

Nagana Gowda GA (2002) Improved sensitivity and gradient-enhanced multiplicity edited two-dimensional heteronuclear shift correlation technique. Chem Phys Lett 353:49–54. https://doi.org/10.1016/S0009-2614(01)01480-4

Otting G, Wüthrich K (1988) Efficient purging scheme for proton-detected heteronuclear two-dimensional NMR. J Magn Reson 76:569–574. https://doi.org/10.1016/0022-2364(88)90361-7

Pantoja-Uceda D, Santoro J (2008) Amino acid type identification in NMR spectra of proteins via b- and g-carbon edited

experiments. J Magn Reson 195:187–195. https://doi.org/10.1016/j.jmr.2008.09.010
Rios CB, Feng W, Tashiro M, Shang Z, Montelione GT (1996) Phase labeling of C-H and C-C spin-system topologies: application in constant-time PFG-CBCA(CO)NH experiments for discriminating amino acid spin-system types. J Biomol NMR 8:345–350. https://doi.org/10.1007/BF00410332
Sakhaii P, Bermel W (2015) A different approach to multiplicity-edited heteronuclear single quantum correlation spectroscopy. J Magn Reson 259:82–86. https://doi.org/10.1016/j.jmr.2015.07.006
Santoro J, King GC (1992) A constant-time 2D overbodenhausen experiment for inverse correlation of isotopically enriched species. J Magn Reson 97:202–207. https://doi.org/10.1016/0022-2364(92)90250-B
Schmidt JM, Rueterjans H (1990) Proton-detected 2D heteronuclear shift correlation via multiple-quantum coherences of the type I_2S. J Am Chem Soc 112:1279–1280. https://doi.org/10.1021/ja00159a077
Schubert M, Labudde D, Leitner D, Oschkinat H, Schmieder P (2005) A modified strategy for sequence specific assignment of protein NMR spectra based on amino acid type selective experiments. J Biomol NMR 31:115–128. https://doi.org/10.1007/s10858-004-8263-z
Schubert M, Oschkinat H, Schmieder P (2001a) MUSIC, selective pulses, and tuned delays: amino acid type-selective ^{1}H–^{15}N correlations, II. J Magn Reson 148:61–72. https://doi.org/10.1006/jmre.2000.2222
Schubert M, Oschkinat H, Schmieder P (2001b) MUSIC and aromatic residues: amino acid type-selective ^{1}H–^{15}N correlations, III. J Magn Reson 153:186–192. https://doi.org/10.1006/jmre.2001.2447
Schubert M, Smalla M, Schmieder P, Oschkinat H (1999) MUSIC in triple-resonance experiments: amino acid type-selective ^{1}H–^{15}N correlations. J Magn Reson 141:34–43. https://doi.org/10.1006/jmre.1999.1881
Shaka AJ, Barker PB, Freeman R (1985) Computer-optimized decoupling scheme for wideband applications and low-level operation. J Magn Reson 64:547–552. https://doi.org/10.1016/0022-2364(85)90122-2
Tashiro M, Rios CB, Montelione GT (1995) Classification of amino acid spin systems using PFG HCC(CO)NH-TOCSY with constant-time aliphatic ^{13}C frequency labeling. J Biomol NMR 6:211–216. https://doi.org/10.1007/BF00211785
Tate S, Masui Y, Inagaki F (1991) Application of the DEPT sequence to the separation of ^{15}NH and $^{15}NH_2$ resonances in ^{1}H-detected ^{15}N single-quantum coherence spectroscopy. J Magn Reson 94:625–630. https://doi.org/10.1016/0022-2364(91)90152-J
van de Ven FJM, Philippens MEP (1992) Optimization of constant-time evolution in multidimensional NMR experiments. J Magn Reson 97:637–644. https://doi.org/10.1016/0022-2364(92)90045-9
Van Melckebeke H, Simorre JP, Brutscher B (2004) Amino acid-type edited NMR experiments for methyl-methyl distance measurement in 13C-labeled proteins. J Am Chem Soc 126:9584–9591. https://doi.org/10.1021/ja0489644
Vuister GW, Bax A (1992) Resolution enhancement and spectral editing of uniformly ^{13}C-enriched proteins by homonuclear broadband ^{13}C decoupling. J Magn Reson 98:428–435. https://doi.org/10.1016/0022-2364(92)90144-V
Walinda E, Morimoto D, Shirakawa M, Sugase K (2017) F_1F_2-selective NMR spectroscopy. J Biomol NMR 68:41–52. https://doi.org/10.1007/s10858-017-0113-x
Williamson MP (2013) Using chemical shift perturbation to characterise ligand binding. Prog Nucl Magn Reson Spectrosc 73:1–16. https://doi.org/10.1016/j.pnmrs.2013.02.001
Zuiderweg ERP (2002) Mapping protein-protein interactions in solution by NMR spectroscopy. Biochemistry 41:1–7. https://doi.org/10.1021/bi011870b
Zwahlen C, Legault P, Vincent SJF, Greenblatt J, Konrat R, Kay LE (1997) Methods for measurement of intermolecular NOEs by multinuclear NMR Spectroscopy: Application to a bacteriophage l N-peptide/*boxB* RNA complex. J Am Chem Soc 119:6711–6721. https://doi.org/10.1021/ja970224q